PROJECT REPORT

On

CONSTRUCTION OF g-C_3N_4/$CuCo_2O_4$ HETEROJUNCTION FOR ENHANCED PHOTOCATALYTIC PERFORMANCE

Submitted by

SAMVRITHA AJITH
(AB23CHE011)

In partial fulfillment for the award of the

Bachelor's Degree in Chemistry

DEPARTMENT OF CHEMISTRY AND CENTRE FOR RESEARCH

ST. TERESA'S COLLEGE (AUTONOMOUS)
ERNAKULAM

2025-2026

DEPARTMENT OF CHEMISTRY AND CENTRE FOR RESEARCH

ST. TERESA'S COLLEGE (AUTONOMOUS)

ERNAKULAM

B.Sc. CHEMISTRY PROJECT REPORT

Name	:	SAMVRITHA AJITH
Register Number	:	AB23CHE011
Year of Work	:	2025-2026

This is to certify that the project "**CONSTRUCTION OF g-C_3N_4/$CuCo_2O_4$ HETEROJUNCTION FOR ENHANCED PHOTOCATALYTIC PERFORMANCE**" is the work done by **SAMVRITHA AJITH.**

Dr. Saritha Chandran A.
Head of the Department

Dr. Merin Joseph
Staff-member in charge

ST. TERESA'S COLLEGE (AUTONOMOUS) ERNAKULAM DEPARTMENT OF CHEMISTRY

Submitted to the Examination of Bachelor's Degree in Chemistry

Date: 6/04/26

Examiners: SENJU DEVADEKUTTY

:

DEPARTMENT OF CHEMISTRY AND CENTRE FOR RESEARCH

ST. TERESA'S COLLEGE (AUTONOMOUS)

ERNAKULAM

CERTIFICATE

This is to certify that the project work entitled "**CONSTRUCTION OF g-C_3N_4/$CuCo_2O_4$ HETEROJUNCTION FOR ENHANCED PHOTOCATALYTIC PERFORMANCE**" is the work done by **SAMVRITHA AJITH** under my guidance in the partial fulfilment of the award of the Degree of Bachelor of Science in Chemistry at St. Teresa's College (Autonomous), Ernakulam affiliated to Mahatma Gandhi University, Kottayam.

DR. MERIN JOSEPH
(Project Guide)
Assistant Professor,
Department of Chemistry and
Centre for Research,
St. Teresas's College, Ernakulam

DECLARATION

I hereby declare that the project work entitled "**CONSTRUCTION OF g-C_3N_4/$CuCo_2O_4$ HETEROJUNCTION FOR ENHANCED PHOTOCATALYTIC PERFORMANCE**" submitted to Department of Chemistry and Centre for Research, St. Teresa's College (Autonomous) affiliated to Mahatma Gandhi University, Kottayam, is a record of an original work done by me under the guidance of **Dr. MERIN JOSEPH, ASSISTANT PROFESSOR,** Department of Chemistry and Centre for Research, St. Teresa's College (Autonomous), Ernakulam and this project work is submitted in the partial fulfilment of the requirements for the award of the Degree of Bachelor of Science in Chemistry.

Samvritha

SAMVRITHA AJITH

Acknowledgements

I would like to express my sincere gratitude to all those who contributed to the successful completion of this project work. First and foremost, I acknowledge the divine guidance and blessings that enabled us to carry out and complete this work.

I express my heartfelt thanks to my research guide, Dr. Merin Joseph, Assistant Professor, Department of Chemistry, St. Teresa's College (Autonomous), Ernakulam, for her constant guidance, support, patience, and encouragement throughout the course of this project.

I extend my sincere gratitude to the Principal, Dr. Anu Joseph and Dr. Saritha Chandran A, the Head of the Department, and all the faculty members of the Department of Chemistry for providing the necessary facilities and a supportive academic environment for this work. I am especially thankful to the non-teaching staff of the Department for their timely assistance and cooperation during the experimental work. I also acknowledge the Director for her role in facilitating institutional support.

Finally, I express my deepest gratitude to my family and friends for their constant encouragement, understanding, and support throughout this journey. I thank everyone who has directly or indirectly contributed to the completion of this project.

SAMVRITHA AJITH

Contents

Chapter 1

Introduction

As the global population grows and industrial activities continue to expand, the demand for clean, reliable, and sustainable energy has become one of the most pressing challenges of our time. Our dependence on fossil fuels is driving not only the depletion of these finite resources but also severe environmental consequences, including global warming, climate change, and air pollution. At the same time, water pollution, particularly from persistent contaminants like antibiotics and synthetic dyes such as methylene blue poses serious threats to ecosystems and human health. In this context, the development and application of clean, pollution-free, and renewable energy sources are of immense importance. Among various alternatives, solar energy emerges as a particularly promising resource as it is abundant, inexhaustible, and environmentally friendly. The challenge lies in effectively capturing, converting, and storing this energy. Photocatalysis, a process that mimics natural photosynthesis, offers a compelling route to convert sunlight into chemical energy, enabling the generation of clean fuels such as hydrogen (H_2). Since the pioneering work of Fujishima and Honda in 1972 on photoelectrochemical water splitting, photocatalytic technologies have gained momentum as a sustainable solution for energy production and environmental remediation. A key to the success of photocatalytic systems lies in the choice of semiconductor materials. Recently, two-dimensional (2D) materials like graphene, transition metal dichalcogenides (TMDs), MXenes, and graphitic carbon nitride (g-C_3N_4) have emerged as strong candidates in this

field. Their unique physicochemical properties, such as high surface area, tuneable electronic structures, and excellent optical characteristics, allow them to perform exceptionally well in energy storage, photocatalytic reactions, and pollutant degradation. These materials show great promise in a wide range of applications, from water splitting and CO_2 reduction to wastewater treatment and fuel cell technologies. Among the above mentioned 2D materials, g-C_3N_4 stands out due to its ability to absorb visible light, suitable band edge positions, and ease of synthesis from earth-abundant elements.

1.1 g-C_3N_4 (Graphitic Carbon Nitride)

g-C_3N_4 is a metal-free semiconductor that was discovered in the late 1800s. Liebig reported melamine, melem, melam, and melon, all of which were identified as triazine and/or tri-s-triazine basic constituents. These were α-C_3N_4, β-C_3N_4, pseudo-cubic-C_3N_4, cubic-C_3N_4, and g-C_3N_4. In contrast to alternative kinds of g-C_3N_4, g-C_3N_4 is simple to synthesize, extremely robust, and has an excellent semiconductive property. In 2009, Wang and his colleagues discovered for the first time that g-C_3N_4 might be exploited for H_2 synthesis under solar irradiation. This was a significant advancement for metal-free photocatalysts. After then, a great deal more study was conducted on the g-C_3N_4 semiconductor, and a great deal of articles were published [1].

1.2 Structure of g-C_3N_4

g-C_3N_4 offers a promising high performance due to its hardness, light weight, preparation from easily available starting material, excellent stability at ambient conditions and as it has suitable band gap energy of 2.7 eV and can absorb blue light up to 450 nm. C_3N_4 exists in five different allotropic forms: α-g-C_3N_4, β-g-C_3N_4, graphitic-C_3N_4, cubic-

C_3N_4, pseudo-cubic-g-C_3N_4 and their bandgap is 5.49, 4.85, 4.30, 4.13, and 2.7 eV, respectively. Among them, g-C_3N_4 has the narrowest bandgap and good light absorption [2].

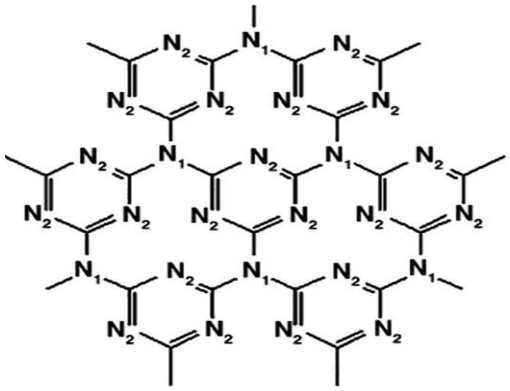

Fig.1 Structure of g-C_3N_4

g-C_3N_4 possesses a stacked 2-dimensional (2D) graphite-like planar structure, with N-heteroatoms substituted in the graphite framework containing p-conjugated systems maintaining a distance of 0.326 nm between two layers. g-C_3N_4 is made up of only carbon and nitrogen and is stable in both acidic and basic media due to the presence of strong covalent bonds between the carbon and nitrogen atoms. Bonding consists of a N-atom (N_1) in a planar sp^2 configuration and a 3-coordinated C-atom, which is sp2 hybridized and is bonded to 2-coordinated N-atom (N_2) in a 1,3,5-triazine ring. Both the nitrogen atoms (labelled as N_1 and N_2) are sp^2 hybridized (Fig. 1) [1].

Inside the molecular building blocks, strong covalent bonds exist, but in the molecular crystal, there exists weak interactions, such as hydrogen bonding and van der Waals forces. Due to the different degree of condensation, the polymerized structure of g-C_3N_4 develops optimization in its packing, which makes the material behave as a multifunctional catalyst. The presence of a pi-conjugated system, as shown in Fig. 2,

modifies its bulk electronic structure and surface properties to allow it to exhibit:

- Electronic properties
- Nucleophilic properties
- The ability to form H-bonds
- Photocatalytic activity

Through its special electronic properties, it can activate the Friedel–Craft reaction, Diels–Alder reactions and trimerization of alkynes. Due to its nucleophilic properties, it helps in the activation of CO_2. Its ability to form H-bonds favors the trimerization of nitrides [1, 3].

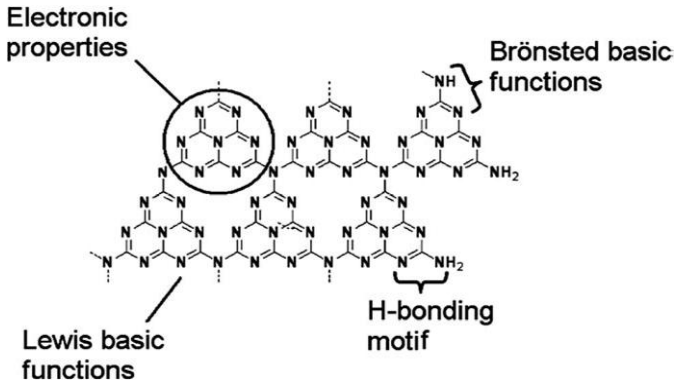

Fig.2 Structure of Planar g-C_3N_4

The appropriate means of selection of precursors and condensation methods had led to two main types of g-C_3N_4 structural polymorphs and this includes, firstly, the g-C_3N_4 consist of a condensed s-triazine units (ring of C_3N_4) with a periodic array of single-carbon vacancies. The second type of g-C_3N_4 consists of the condensed tri-s-triazine (tri-ring of C_6N_7) subunits coupled through planar tertiary amino groups, and this has greater periodic vacancies in the lattice. The g-C_3N_4 networks mainly consists of melon-based segments (the second type structure; this consists

of the tri-s-triazine unit, Fig. 3a) which is thermodynamically more stable compared to the melamine-based arrangements (the first type structure; this compose of the s-triazine, Fig. 3b) as described by the functional theory (DFT) calculations. Hence, it is broadly believed that the tri-s-triazine nucleus is the fundamental building blocks for the formation of the g-C_3N_4 network. Tri-s-triazine (C_6N_7) or triazine (C_3N_3) rings are connected by C-N bonds to form a layered structure with triangular nanopores uniform distribution, which is different from the honeycomb structure closely connected in graphene layers [4].

Fig.3a) Tri-s-triazine and 3b) triazine structures of g-C_3N_4

1.3 Synthesis of g-C_3N_4

g-C_3N_4 can be prepared by Thermal polymerization of precursors such as urea [5], thiourea [6], cyanamide [7], dicyandiamide [8] and melamine [9]. In general, the synthesis of g-C_3N_4 could be divided into two processes: Polyaddition and Polycondensation. Both processes are temperature-dependent. The precursors firstly polymerize to melamine (Polyaddition process). Then Melamine is condensed by the loss of ammonia (polycondensation), which finally results in the formation of g-C_3N_4 polymer [10].

The g-C_3N_4 powder was obtained by heating urea/ Thiourea/ Cyanamide/ Dicyandiamide/ Melamine or we can combine both urea and thiourea in the ratio of (1:1) in microwave muffle furnace. Typically, 20 g of urea was calcined at 550˚C for 2 hours with heating rate of 5˚C min-1. The obtained bulk g-C_3N_4 was collected and ground to powder after cooling. Different kinds of precursors and calcination temperature can greatly affect the physicochemical features of the subsequent g-C_3N_4, including the specific surface area, porosity, absorption edge, photoluminescence, C/N ratio, and nanostructure design [10].

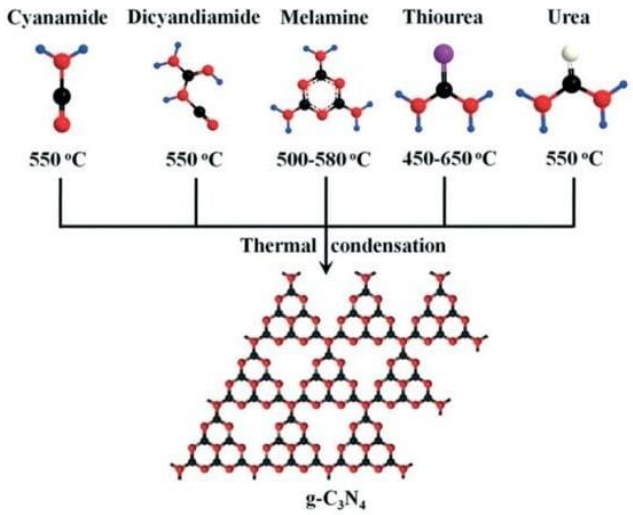

Fig.4 Schematic illustration of the main synthesis routes of bulk g-C_3N_4

The formation of graphitic carbon nitride proceeds by various routes at thermal condensation of the above-mentioned precursors. At thermal pyrolysis, the cyclization of any of the above-mentioned nitrogen-containing precursors yields melamine. The dimerization of melamine at 350°C yields melem and melon that transforms into polymeric g-C_3N_4 at temperatures above 500°C [11]. Graphitic carbon nitride is known to have

a defect-rich structure, which results from incomplete deamination during thermal polycondensation. For this reason, synthesizing high-crystalline g-C_3N_4 is a difficult task, albeit exact crystallinity (correct arrangement of atoms) is a critically important parameter affecting the band structure and charge recombination rate (e-/h+) of a photocatalytically active material. A large number of structural defects increases the charge recombination rate, and thus impedes photocatalyst activity. Texture controlling can improve the chemical, physical, and optical properties of g-C_3N_4 [11].

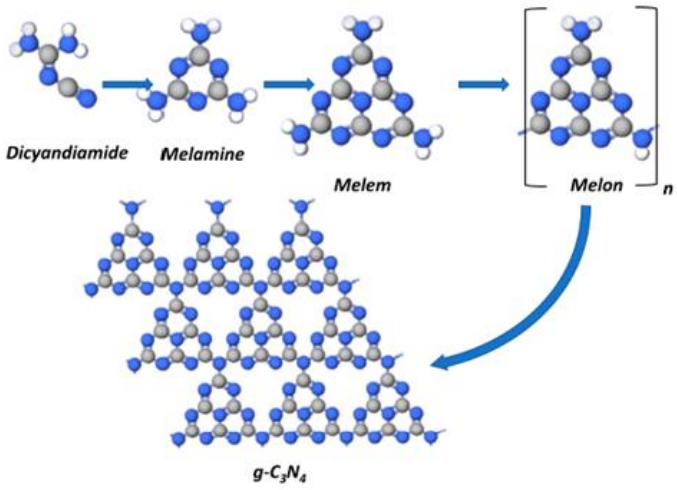

Fig.5 Thermal Condensation of Dicyandiamide to form g-C_3N_4

1.4 Properties of g-C_3N_4

1.4.1 Physical properties:

g-C_3N_4 is an organic n-type semiconductor photocatalyst with a bandgap of 2.7 eV corresponding to visible absorption of 460 nm. The electron-rich nature of g-C_3N_4 enables it to absorb visible light corresponding to a wavelength of 460 nm (pale yellow colour). DFT calculation studies on the band structure of g-C_3N_4 stated that the VB (HOMO) and CB (LUMO)

results from the p_z orbitals of pyridine like nitrogen and carbon p_z orbitals with significant contribution from edge nitrogen atom respectively. The CB and VB edge potentials from Mott-Schottky (M-S) plot and Valence Band X-ray Photoelectron Spectra (VB-XPS) are found to be −1.3 and 1.4 V and −1.53 and 1.16 V respectively vs NHE at pH 7. The slight difference in values is acceptable for an n-type semiconductor like g-C_3N_4. The VB and CB edge potentials are suitable for many photocatalytic redox reactions [12]. It is known for its high thermal and chemical stability. It is one of the highly thermally stable organic compounds and is stable up to 600°C, beyond which oxidation occurs via distinctive C, N fragmentation reactions. Moreover, thermogravimetric analysis (TGA) of g-C_3N_4 revealed a sharp endothermic peak at 630°C, equal to the sequential total weight loss which indicates that the thermal decomposition and vaporization of the samples have commenced at this temperature. The overall decomposition of g-C_3N_4 happens at 750°C, and no remains of the materials are left subsequently. Gillan hermetically sealed g-C_3N_4 in an evacuated silica ampoule and positioned it in a range of different temperatures. The result showed that a very gentle sublimation of g-C_3N_4 occurs at 450°C and a tremendous increase at 650°C. This thermal stability of g-C_3N_4 is the highest among those of characteristic high-temperature organic polymers, which is superb for high-temperature applications. However, the thermochemical stability of g-C_3N_4 is different using different preparation methods, which is affected by the various degrees of polycondensation of the g-C_3N_4 precursors [13].

UV-vis diffuse reflectance spectroscopy and photoluminescence spectroscopy typically characterize the optical features of g-C_3N_4. Optimizing the optical features of g-C_3N_4 is also of immense importance to achieve superior photocatalytic performance. It should be noted that the

physicochemical properties, for instance, the bandgap energy of the state-of-the-art g-C_3N_4 semiconductor photocatalytic material, are correlated with the kind of precursor, condensation temperature, difference in band gap and applications, as shown in Table.1. This difference in bandgap energies is usually related to the formation of different local structures, packing motif, and defects produced in the course of the synthesis or modification procedures. Also, different modifications of g-C_3N_4 may result in a hypsochromic shift (for instance, protonation or Sulphur doping) or a bathochromic shift (B and F doping and copolymerization with malonylurea). The favourable electronic band structure also makes the g-C_3N_4 photocatalyst suitable for applications related to photoelectrochemical and solar energy conversion. Moreover, modification in the nanostructure of g-C_3N_4 results in a tuned electronic band structure and improved photocurrent response. For instance, mesoporous g-C_3N_4 can enhance the light harvesting capacity due to its larger specific surface area and multiple light-scattering effects, and consequently exhibit an improved electrical conductivity [13].

Precursors	**Temperature (in°C)**	**Band Gap (eV)**	**Application**
Urea	450-550	2.7	Water splitting
Thiourea	450-650	2.4-2.6	Organic Pollutant Degradation
Dicyandiamide	450-550 >600 (Collapse)	2.7-2.8	Bacterial Inactivation
Cyanamide	550	2.7-2.8	Photoelectrochemical devices
Dicyandiamide under H_2	450-550	2.5-2.6	Hydrogen Production
Cyanamide under CO_2	500-580	2.4-2.5	CO_2 photoreduction to fuels (CH_4,CO)
Melamine	500-580	2.8-3.0	Fluorescent sensors[14]

Table. 1 Synthesis Parameters, Properties and Applications of g-$_3N_4$

1.5 Modifications of g-C_3N_4

Pristine graphitic carbon nitride (g-C_3N_4) is a promising metal-free semiconductor, but its use in photocatalysis is limited by a few key issues. The main problems are that its electrons and holes tend to recombine quickly, and its bandgap is too wide to absorb much visible light [15]. Carbon nitride, albeit known for a long time, has been tested as a photocatalyst only since 2009. Every year, the interest of researchers in this material increases, about 10–12% of all studies on the photocatalytic H_2 production devoted to the synthesis and study of photocatalysts based on g-C_3N_4 and their applications. Graphitic carbon nitride g-C_3N_4 has the band gap of 2.7 eV and the conduction band-edge potential -1.3 V vs. NHE, which enables an efficient hydrogen production process. The downside of this process is that it yields materials with low specific surface areas and high electron-hole recombination rates that provokes the loss in the catalytic activity. To stabilize the photocatalytic activity of g-C_3N_4, the following approaches are used:

1. Alteration of textural characteristics by introducing templates, pore formers, or pre-treatment method;
2. Doping with heteroatoms [16-18]
3. Modification with metals
4. Construction of composite photocatalysts.

The following strategies are used for the modifications of g-C3N4:-

1.5.1 Elemental Doping: Doping in semiconductor photocatalyst is generally a band engineering strategy by virtue of which the bandgap reduction and extended absorption towards the visible region of the solar spectrum occur. In the case of g-C_3N_4, various elemental (metal or non-metal) and molecular (copolymerization with organic moieties) doping has emerged to improve the photophysical properties in the last

few years. Elemental doping is in accordance with the ionic radii of the dopant and the in-planar and inter planar distance between the C_3N_4 lattices, thereby resulting in substitutional or interstitial doping [12].

***1.5.2 Metal Doping*:** Metal doping generally takes place by the insertion of metal atoms into the C_3N_4 framework via cave doping, in which metal atoms get fixed into the large nitride pores (pots) of triazine units by the strong electrostatic attraction between negatively charged nitrogen and the positive metal cations. The reduction in bandgap is achieved via the introduction of additional energy levels by metallic impurities, which may be lower or higher than the CB minimum and VB maximum, respectively, to reduce the bandgap values. Many alkali/alkaline earth metals, transition metals or noble metals are incorporated into the C_3N_4 matrix by adding soluble salts during thermal condensation polymerization [12].

1.5.3 Alkali/Alkaline Earth Metal Doping: Cave doping alkali metal cation induces non-uniform spatial charge distribution in different directions and thereby enhance charge transfer kinetics [19] and an increased number of charge carriers. The combined effect of dopants and structural oxygen atoms strongly influences the material's morphology and band structure. Besides, there is a reduction in the doped system's surface area values due to the agglomeration of doped C_3N_4 and limited CO_2 release during thermal condensation [12].

1.5.4 Noble Metal Doping: An interesting study based on DFT calculations indicated that the cave doping of noble metals like Pd, Pt in semiconductor material would reduce the optical bandgap, thereby facilitating extended visible light absorption. These are the outcome of surface plasmon resonance (SPR) and Schottky barrier (space–charge separation region) generation. The nano Ag deposition on C_3N_4 sheets leads to increased surface area [20], and all these factors positively

influenced the TC degradation. Porous C_3N_4 (PCN) decorated with Ag nanoparticles for the degradation of TC was reported. PCN/Ag composites have superior surface area value (100 m^2/g) and reduced bandgap (2.68 eV) [21], which results in improved TC degradation kinetics. They have used Pt decorated C_3N_4 for the simultaneous degradation of macrolide antibiotic and hydrogen production [22], in which macrolide act as a sacrificial agent and being consumed in the reaction. Au/Pt/g-C_3N_4 plasmonic photocatalyst for TC HCl degradation was one of the first reports on antibiotic degradation by C_3N_4 based systems [12].

1.5.5 Other Transition/Inner Transition Metal Doping: Apart from noble metals, other transition metals are also cave doped into nitride pores of triazine units of C_3N_4 enabling superior photophysical properties. Single atom such as Co loaded in C_3N_4 matrix is achieved through a bidentate ligand approach. Interestingly, an interlayer and intralayer Cu doping on the C_3N_4 matrix was reported for the degradation of Norfloxacin (NOR) antibiotic [23, 24]. Porous C_3N_4 with Cu(I) ions with traces of Cu_2O is reported for the degradation of chlortetracycline hydrochloride (CTC HCl) via metal to ligand charge transfer (MLCT) phenomena. Fe^{3+} doped porous C_3N_4 for the degradation of sulfadiazine antibiotic [25] is reported by Ou et al. Doping of rare earth metal ions on C_3N_4 gathered interest due to the availability of unfilled 4f orbital and empty 5d orbital, which serves as electron capturing centre to improve the photoinduced charge carrier and restrict the recombination rate. Mesoporous C_3N_4 doped with Sm for TYL degradation via simple one step calcination are realized [12].

1.5.6 Non-Metal (Anion) Doping: Generally, non-metal doping in C_3N_4 occurs by the chemical substitution leading to reduced bandgap and enhanced visible light absorption. Copolymerization of dicyandiamide with ammonium citrate in a one-step thermal polymerization leads to

carbon doped C_3N_4 with some nitrogen vacancies [26]. The electrical conductivity and charge transfer separation is greatly enhanced by the replacement of bridging nitrogen. A red shift in bandgap is observed due to the improved π–π* and n–π* transitions as proven by DFT calculations. In a notable work, Guo et al. introduced a one-step strategy for Cl doping in C_3N_4 nanosheets for the degradation of tetracycline [27]. C_3N_4 doped with Cl and Br using NH_4Cl and NH_4Br respectively is reported for oxytetracycline degradation in a similar approach. The acid gas like HCl/HBr gas leads to doping in C_3N_4 sheets and protonation; both improve the photocatalytic performance [12].

1.5.7 Co-Doping (Anion+Anion): Co-doping of anions has recently attracted much interest in the field of semiconductor photocatalysis by the synergistic effects of dopants compared to single dopant. Recently, a one-step thermal polymerization of polyvinylpyrrolidone (PVP), guanidinium hydrochloride (GndCl) and hexachlorotriphosphazene (HCCP) for the fabrication of P and O co-doped C_3N_4 is reported [28] for the degradation of a number of fluoroquinolone antibiotics. Based on the various spectroscopic techniques like XPS and NMR, it is found that the corner and bay carbon atoms are replaced by P atoms while, oxygen is occupied in the place of N in the C_3N_4 framework. Another report on P-Cl co-doped C_3N_4 with nitrogen-vacancy emphasised the degradation of norfloxacin [12].

1.5.8 Metal/Non-Metal Co-Doping: The synergy between metal and nonmetal dopants is a way to improve the photophysical properties of photocatalysts. In a recent paper, C Ce co-doped porous C_3N_4 prepared by supramolecular self-assembly is reported for the TC degradation. Another report on S and Gd co-doped C_3N_4 exhibited better photocatalytic degradation of sulphamethazine (72%/180 min) compared to pristine C_3N_4

(10%/180 min). Similarly, K & I and Ag & P co-doped C_3N_4 are widely reported for antibiotic degradation [29]. Nguyen et al. fabricated Ag P co-doped C_3N_4 for the degradation of sulphamethoxazole [30]. The bandgap reduction and effective separation of exciton lead to 99% degradation of antibiotic [31] within 30 min of visible light irradiation [12, 30].

1.5.9 Heterojunction interfaces: Concurrent charge separation and migration of photo generated charge carriers are two important factors that will define the overall photocatalytic activity. The charge separation in single component photocatalyst is sometimes inadequate for large scale applications. The construction of heterojunction interfaces between two or more compatible components (semiconductor/metal/non-metal) is an advanced technique to ensure the effective separation and migration of electron-hole pairs in semiconductor photocatalysis. The alignment of band structures of two different semiconductors results in the formation of heterojunction. The junction formation results in a band bending phenomenon, leading to the built-in electric field in the space charge region. As a result, the migration of electrons and holes occurs in the opposite direction and promotes spatial charge separation and reduces the recombination rates [32]. The creation of junction is influenced by the electronic structure, electron affinity, and work function of the participating materials. Based on the phase composition, heterojunctions can be classified as isotype or hetero type junctions [12]. The interface formed between different compounds is generally termed as hetero type junctions or simply heterojunctions. Hetero type junction can be classified in different ways according to the number of components or depending on the band alignment of the components. Considering the number of components, the heterojunctions can be classified further into binary, ternary, or quaternary heterojunctions. The important heterojunctions

based on band alignments are type I, type II, type III, Schottky, p-n and Z-scheme. The confinement of VB and CB of small bandgap material within the large bandgap material leads to a straddling kind arrangement of band edges, which is termed as type I heterojunction. In type II heterojunction, a staggered band alignment of the semiconductor offers effective separation of the charge carriers by the creation of a built-in electric field on account of the chemical potential difference of the band edges. Type II heterojunction provides more room for extended visible light absorption, fast charge migration, reduced exciton recombination, and shows enhanced photocatalytic performance. A broken type of arrangement of band edge positions without band crossing is observed in type III heterojunction [12].

These heterojunctions are very rare, and thus reports of such junctions displaying effective results are also rare. A conventional Z-scheme photocatalysis is defined by a two-step photoexcitation process as similar to natural photosynthesis. It comprises two photocatalysts and an electron acceptor-donor pair. In a photocatalysis process, the Z-scheme heterojunction comprises one photocatalyst with strong reductive electrons and another photocatalyst with strong oxidative holes, aiding spatial charge separation and thereby improving the photocatalytic activity. The photocatalytic activity of all-solid-state Z-scheme enhances the overall spatial charge separation of electron–hole pairs [12, 33].

1.6 Spinel Oxides and Catalytic Activity

To improve its photocatalytic activity, composites of g-C_3N_4 with other semiconductor materials are formed. Among these, spinel structured compounds such as $ZnCo_2O_4$, $NiCo_2O_4$, $CuAl_2O_4$, $CuCr_2O_4$, $ZnCr_2O_4$, $MnCo_2O_4$, and $CuCo_2O_4$ gained more attention due to their incredible

applications in electronic, magnetic, catalytic, sensing reduction of organic molecules, electrocatalyst for oxygen evolution reaction, and anode materials. The combination of high electrochemical activity, interconnected nanostructured morphology, and the presence of multiple redox-active sites contributes to their higher energy storage and oxygen evaluation performance [34].

1.6.1 Copper Cobaltite (CCO)

$CuCo_2O_4$ stands out due to its unique spinel structure, which enables rich redox chemistry and superior electrochemical activity. Unlike binary oxides such as Co_3O_4, CuO, or NiO; $CuCo_2O_4$ benefits from the synergistic interaction between Cu and Co ions, which enhances charge transport, catalytic efficiency, and active site density. $CuCo_2O_4$ features a spinel AB_2O_4 structure, with A as the bi-valent Cu metal atom on tetrahedral sites and Co as the tri-valent transition metal atom on octahedral sites. Additionally, $CuCo_2O_4$ exhibits higher electrical conductivity and better cycling stability than many other transition metal oxides, making it a promising candidate for high-performance applications in energy storage, electro-photocatalysis, optoelectronic devices, electrochemical sensors, solar cells and biomedical applications. Its substantial active surface area and conductivity enhance the charging and discharging processes, essential for energy storage devices. Furthermore, its catalytic activity in oxygen evolution (OER), hydrogen evolution (HER), oxygen reduction reaction (ORR), and CO_2 photoreduction [35-37] plays a crucial role in electrochemical processes such as water splitting [38-40] and fuel cells. The wide bandgap and capability to absorb a broad spectrum of visible and near-infrared light render it effective for solar energy harvesting. Beyond its notable electrochemical and catalytic

response, $CuCo_2O_4$ has recently gained attention in biomedical applications due to its unique physicochemical properties. Specifically, $CuCo_2O_4$ nanoparticles have been explored for their antibacterial properties, because of their ability to generate reactive oxygen species (ROS) and the release of Cu^{2+} and Co^{2+} ions [41].

In order to enhance the photocatalytic properties, coupling of p and n-type semiconductor materials like $CuCo_2O_4$ (p-type) or g-C_3N_4 (n-type) will be more appropriate. The fabricated $CuCo_2O_4$/g-C_3N_4 (1:0.5), $CuCo_2O_4$/g-C_3N_4 (1:1) and $CuCo_2O_4$/g-C_3N_4 (1:2) composite catalysts were tested for MO degradation under solar light illumination. Compared to the bare $CuCo_2O_4$ and g-C_3N_4, the photocatalytic performances of hybrid composites were found to be low due to the shielding of $CuCo_2O_4$ over g-C_3N_4 which reduces the absorption capacity of g-C_3N_4 and also the surface area lower than bare photocatalysts. The addition of H_2O_2 increases the degradation process which might be due to the decomposition of H_2O_2 and the production of hydroxyl radicals (•OH) on the catalyst surface facilitates the reaction process faster [41]. The photocatalytic degradation of these pollutants results from the generation of reactive species such as h^+, H_2O_2, •OH and O_2^-•. Electrons and holes produced under sunlight within the excited $CuCo_2O_4$ allow absorbed oxygen molecules to trap electrons forming superoxide radicals O_2^-•. These active species act as oxidants, degrading various pollutants such as carbonyl, amino, hydroxyl groups, among others [42].

1.7 Photocatalytic Degradation of Antibiotics

Ciprofloxacin (CIP) is a fluoroquinolone group broad-spectrum antibiotic drug that can act as a bidentate ligand forming iron complexes during its

degradation in the photo-Fenton process (PFP). It works through the inhibition of protein synthesis of both gram-positive and gram-negative bacteria. CIP was globally prescribed in the order of 18.7 million defined daily doses in the year of 2010 (Schwabe and Paffrath, 2011). CIP could exist in target organisms even up to 72% of non-metabolized forms (Ternes, 2003). In a bulk drug production site in Patancheru, Hyderabad (India), the concentration of CIP obtained in disposed water was as high as the toxicity limit to some bacteria (Larsson et al., 2007). In fact, CIP residues are frequently found in hospital wastewater, sewage treatment plant effluent, and surface water (Li et al., 2011). CIP molecules also have a strong tendency to be adsorbed on sewage sludge (Golet et al., 2002) [43].

Fig.6 Structure of CIP

Ciprofloxacin is a solid white powdery compound having half-life of about 3–4 hours. Figure 1 shows the structure of ciprofloxacin. In order to avoid its photodegradation, it is stored in dark at 4°C. It has a melting point of 255–257°C and solubility is dependent on pH; at pH below 5 the solubility is maximum and minimum when pH is near 7, i.e., isoelectric point (Sharma et al., 2017). This drug has a concentration-dependent permeability and passes through most of the body tissues and fluids well

such as bile, prostatic tissues, gingival fluid, and lungs (Sharma et al., 2017) [44].

In a recent study, the degradation of Ciprofloxacin (CIP) was reported by a novel p-n junction created by nitrogen-deficient g-C_3N_4 loaded with polyoxometalate porous photocatalysts. The nitrogen-deficient nanosheets of carbon nitride were prepared by the magnesium thermal denitrification process. The addition of Mg powder along with melamine as the raw component results in formation of black porous structures of g-C_3N_4 [12]. The g-C_3N_4/$CuCo_2O_4$ heterojunction effectively degrades the antibiotic CIP by creating a highly efficient Z-scheme photocatalytic system.

When exposed to light, this system boosts the separation of charge carriers, preventing them from simply recombining. Under illumination, electrons from the $CuCo_2O_4$ conduction band migrate to combine with holes in the g-C_3N_4 valence band. This unique pathway preserves the electrons with high reductive power on g-C_3N_4 and the holes with strong oxidative power on $CuCo_2O_4$. These separated, powerful charges then react with oxygen and water to generate a high concentration of reactive oxygen species (ROS), specifically superoxide radicals ($\bullet O^{2-}$) and hydroxyl radicals (•OH). These highly reactive radicals are the key agents that attack and mineralize the complex structure of the Ciprofloxacin molecule, breaking it down into less harmful byproducts.

Objectives

Synthesis and optimization of graphitic carbon nitrite(g-C_3N_4) from urea and thiourea precursors

Synthesis of $CuCo_2O_4$ spinel type cobaltite.

Fabrication and characterization of g-C_3N_4/$CuCo_2O_4$ cobaltite heterostructure.

Evaluation of Photocatalytic performance using Ciprofloxacin (Antibiotic) degradation.

Chapter 2

Materials and Methods

This chapter gives a brief description of the materials and experimental procedures adopted for the present investigation.

2.1 Materials Required

- Urea
- Thiourea
- Copper Nitrate
- Cobalt Nitrate
- Sodium Hydroxide
- Distilled water

2.2 Apparatus Required

- Silica crucible
- Magnetic Stirrer
- Muffle furnace
- UV-Vis lamp

2.3 Experimental Procedures

2.3.1 Preparation of g-C_3N_4

The graphitic carbon nitride samples were synthesized via a direct thermal polycondensation method using urea and thiourea as precursors. In a typical synthesis, 10 g of the precursor (urea, thiourea, and a 1:1 mass ratio mixture of both - hereafter denoted as CNU, CNT and g-CN respectively) was placed in a covered silica crucible separately. The crucible was heated in a muffle furnace in a Temperature of 500℃ - 550℃. The sample was calcined at this temperature for 1 hour in an air atmosphere. After the heating process, the furnace was allowed to cool naturally to room temperature. The resulting product, obtained as a pale-yellow solid, was collected and ground into a fine powder for further physicochemical characterization [45].

2.3.2 Synthesis of Copper Cobaltite

The Spinel shaped Copper Cobaltite (CCO) can be synthesized using a co-precipitation - 550℃ annealing method. In the first step, 3 mmol of copper nitrate and 6 mmol of Cobalt nitrate were dissolved in 25 mL of deionized water. Simultaneously, 22.5 mmol of NaOH was dissolved in another 25 mL of deionized water. The two solutions were then mixed under stirring. The mixture was stirred in a water bath at 60°C for 30 minutes and then aged at room temperature for 2 hours. In the second step, the reaction mixture was centrifuged at high speed to obtain the solid product, which was then washed and centrifuged multiple times. In the third step, the purified solid product was placed in a tube furnace and annealed at 550°C for 3 hours in an air atmosphere, with a heating rate of 5°C per minute, to obtain the $CuCo_2O_4$ solid powder [46].

2.3.3 Preparation of $CuCo_2O_4$/g-C_3N_4 Hybrid Composites - Impregnation Method

An impregnation strategy was adopted for the preparation g-C_3N_4/$CuCo_2O_4$ hybrids. In a typical process, 0.5 g g-C_3N_4 was dispersed in ethanol via stirring. An ethanolic solution of $CuCo_2O_4$ was added to the above solution and further stirred for 12 hours followed by solvent evaporation under continuous stirring and heating. The samples were dried at 80˚ C for 8 hours. A g-C_3N_4/$CuCo_2O_4$ hybrids with 5 weight percentage of $CuCo_2O_4$ was synthesized and denoted hereafter as g-CN/CCO [47].

2.4 Photocatalytic Studies

The photocatalytic activity under visible light irradiation of the as-prepared g-C_3N_4 samples from different precursors was assessed using the photocatalytic degradation of methylene blue [48]. The percentage degradation of methylene blue was assessed by monitoring the absorbance of the solution at 664nm at definite time intervals.

2.5 Photocatalytic Degradation Ciprofloxacin

The application of studies of the hybrid samples were conducted. The samples were used for the degradation of the antibiotic ciprofloxacin. In a single run, 10 mg of the catalyst was dispersed in 10 ml of the aqueous solution of ciprofloxacin (10 mg/L) and the suspension was stirred in the dark to attain the adsorption/desorption equilibrium. The percentage degradation of CIP was assessed by monitoring the absorbance of the solution at 268 nm at definite time intervals

2.6 Characterization Techniques

2.6.1 Fourier Transform Infrared Spectroscopy (FTIR)

Infrared (IR) spectroscopy, particularly Fourier Transform Infrared Spectroscopy (FT-IR), is a widely used technique for chemical analysis in laboratories. It provides valuable insights into molecular vibrations, enables the identification of functional groups within a molecule making it a powerful tool for recognizing the chemical composition of a compound.

The method is based on the absorption of infrared light by a sample, resulting in a spectrum that displays absorbance or transmittance intensity against frequency (wavenumber). Each peak in the IR spectrum corresponds to specific molecular vibrations, allowing for the identification of functional groups. As such the IR spectrum acts as a unique fingerprint for unknown compounds, which can be compared with standard reference spectra for structural identification. IR spectroscopy is versatile and can be used to analyze both organic compounds and inorganic materials, such as minerals and metals. Additionally, it can be applied to liquids and solids at atmospheric pressure.

2.6.2 X-Ray Diffraction (XRD)

XRD is a non-destructive analytical technique used primarily for characterizing crystalline materials. An XRD instrument measures the intensity of the diffracted X-rays as a function of the scattering angle (2^{θ}). This produces a diffraction pattern-a plot of intensity versus 2^{θ}. The positions of peak in the pattern is determined by the spacing between the atomic planes and therefore reveals the size and shape of the unit cell and the arrangement of atoms within the compound. As a result, the X-ray

diffraction pattern serves as a fingerprint for the periodic atomic arrangement present in a material.

2.6.3 Field-Emission Scanning Electron Microscope (FESEM):

Field Emission Scanning Electron Microscopy (FESEM) is an advanced surface characterization technique used to observe the morphology, topography, and size distribution of materials at very high resolution. Actually Field Emission indicates the type of electron gun used. Field Emission is one of the different types of electron gun used in SEM system. The fundamental principle is similar to conventional Scanning Electron Microscopy (SEM), where a focused electron beam scans the specimen surface, and signals generated from electron sample interactions (primarily secondary electrons) are collected to form a high magnification image.

2.6.4 Ultraviolet-Visible Reflectance Spectroscopy (UV-DRS):

UV-DRS is a non-destructive technique used to analyze the optical properties of solid materials, particularly their absorption and reflection of UV and visible light. This method is valuable for characterizing electronic properties, determining bandgaps and other surface properties of materials like semiconductors, catalysts, and pigments.

Chapter 3

Results and discussion

3.1 Characterization of g-C_3N_4 and g-C_3N_4/$CuCo_2O_4$

3.1.1 XRD

Crystallinity and phase purity of the samples were ensured by XRD analysis. The pure g-C_3N_4 exhibits two characteristic peaks at 13.0˚ and 27.6˚ corresponding to the (100) and (002) planes. The high intensity peak at 27.6˚ corresponding to an interlayer d-spacing of 0.321 nm can be attributed to the periodic stacking of layers of 2D graphitic systems. The comparatively weak peak at 13.0˚ corresponds to an interlayer spacing of 0.678 nm which is due to the in-plane trigonal nitrogen linkage of tri-s-triazine motifs. No discernible impact could be observed in the XRD pattern upon insertion of $CuCo_2O_4$, indicating the preservation of the framework. The absence of distinctive peaks corresponding to $CuCo_2O_4$ or any shift in the inherent peaks of g-C_3N_4 may be relatively low content and fine dispersion of $CuCo_2O_4$ on 2D layers [49].

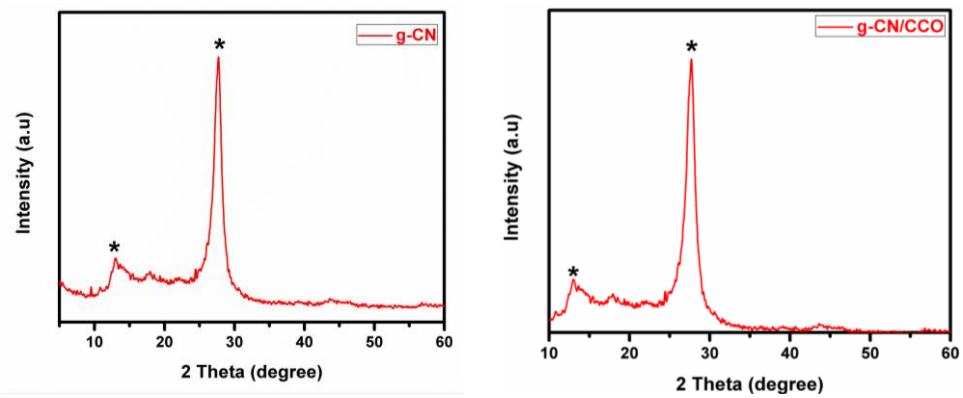

Fig.7 XRD Patterns of g-CN and g-CN/CCO

3.1.2 FESEM

These are the FE-SEM images of gCN and its composite gCN/CCO. This analysis reveals that the synergestic dispersion of g-C_3N_4 sheets and porous $CuCo_2O_4$ provides superior distribution and well mixed composite photocatalysts. Therefore, we expected that such a gCN/CCO hybrid structure is beneficial for improving the absorption of light, adsorption of dyes and transfer the photoexcited electrons [49].

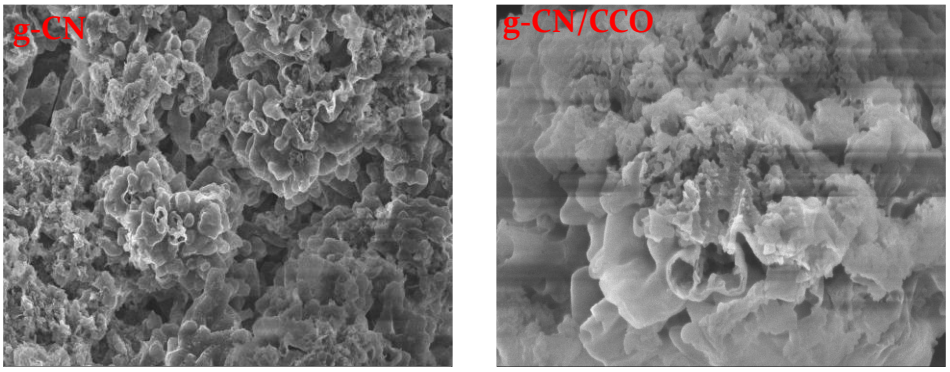

Fig.8 FESEM images of g-CN and g-CN/CCO

3.1.3 FTIR

The surface functionalities of g-C_3N_4 and g-C_3N_4/$CuCo_2O_4$ hybrid systems were analyzed by FTIR spectroscopy. The broad peak observed in the range 3000–3500 cm^{-1} could be ascribed to N–H stretching vibration of terminal amino groups and may also have the contribution of O–H from adsorbed moisture. The characteristic peaks of g-C_3N_4 exist in the range of 1200–1700 cm^{-1}. The peaks at 1227, 1429, 1572, and 1644 cm^{-1} represent the characteristic skeletal vibrations of aromatic CN heterocycles. A peak at 810 cm^{-1} is observed, which is typical of out-of-plane bending of tris-s-triazine units. The conservation of the parent structure of g-C_3N_4 is affirmed by the FTIR spectra as the spectra of g-C_3N_4/$CuCo_2O_4$ retained

all the intrinsic peaks of g-C_3N_4. Further, New small peaks at ~500-700 cm^{-1} indicate the presence of Co-O bonds from the cobalt oxide [49].

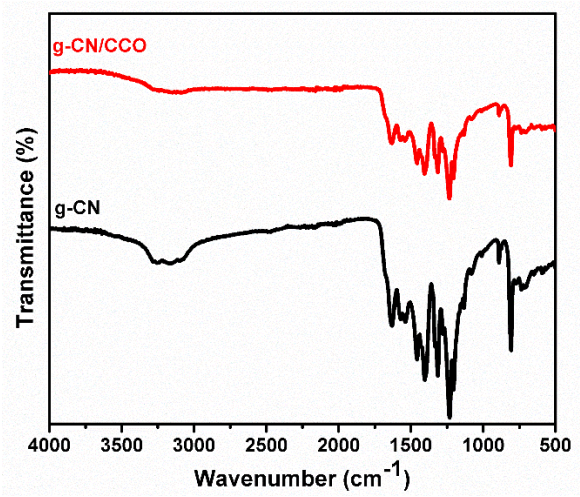

Fig.9 FTIR Spectra of g-CN and g-CN/CCO

3.1.4. UV-DRS

a) ***b)***

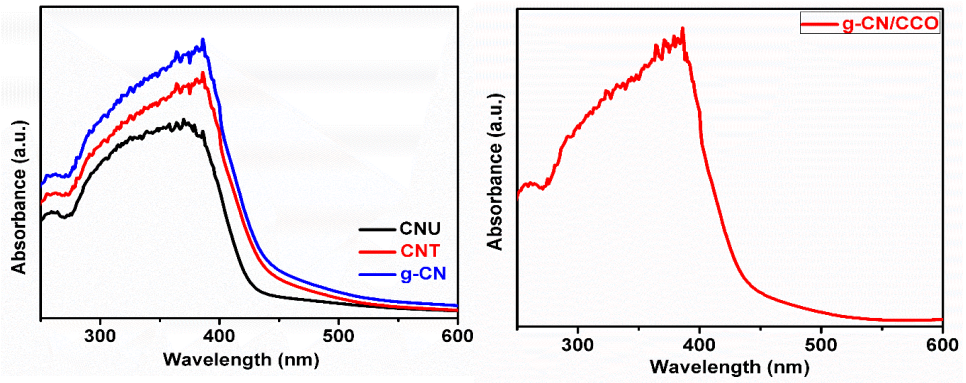

Fig.10a) UV-DRS Spectra of CNU, CNT, g-CN 10b) UV-DRS Spectra of g-CN/CCO Composite

3.2 Photocatalytic Studies

To optimize the combination of precursors, three different trials were conducted. Three different types of carbon nitrides were synthesized using urea, thiourea and 1:1 combination of urea and thiourea. The sample prepared with the combination of urea and thiourea named as g-CN showed maximum absorption in UV-DRS spectra. In order to further substantiate the results, the photocatalytic activity of the samples was compared. For this, the degradation of methylene blue was selected as a model reaction. In the reaction the g-CN sample exhibited pronounced activity for methylene blue degradation followed by CNT and then CNU. The reaction was conducted under visible light irradiation. The progress of the reaction was monitored using UV-Vis spectrophotometer. The concentration of methylene blue was 10 ppm. The UV profile and comparison of degradation percentages are given in fig. 11a and 11b.

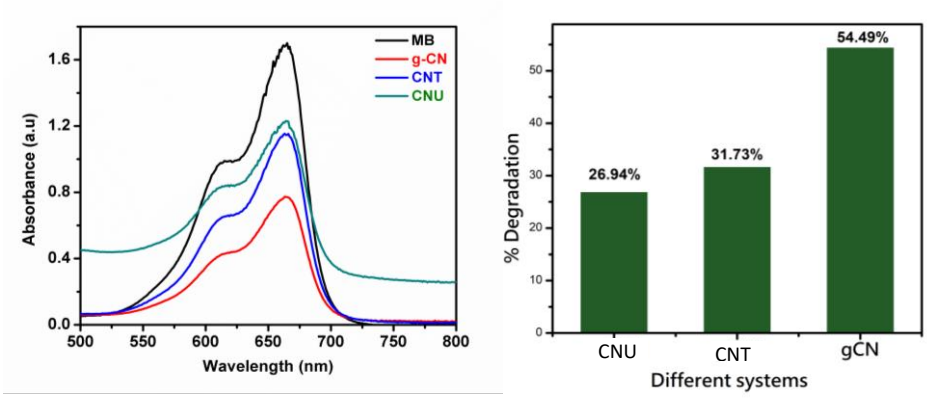

Fig.11a) UV-Vis Spectra of CNU, CNT and g-CN in Degradation of Methylene Blue 11b) Comparative Evaluation of Photocatalytic Performance.

3.2.1 Photocatalytic Degradation of Ciprofloxacin

The application of as prepared hybrid systems was assessed using the degradation of an antibiotic CIP. The self-photolysis of CIP assessed in the absence of catalyst indicated negligible response. Prior to light exposure, the CIP solution containing the catalyst was placed in the dark for 30 min under continuous stirring to establish the adsorption desorption equilibrium. The solution was then exposed to visible light irradiation and percentage degradation was calculated from the change in the absorbance of CIP solution at 268 nm before and after irradiation. After 60 min of irradiation, the percentage degradation observed with various catalyst systems is depicted in first Figure.12a. Incorporation of $CuCo_2O_4$ enhanced the Photocatalytic activity, maximum performance being displayed by g-C_3N_4/CCO which could be attributed to better charge transfer prospects due to the synergistic heterojunction architecture. Spectroscopic analysis revealed a gradual decrease in the absorbance of CIP with time indicating slow degradation. A comparative evaluation of absorption spectra shows almost complete degradation of CIP within 2 h in the presence of g-C_3N_4/CCO. Concentration–time plots also supplement the slow degradation of CIP, as indicated in spectral studies.

a) **b)**

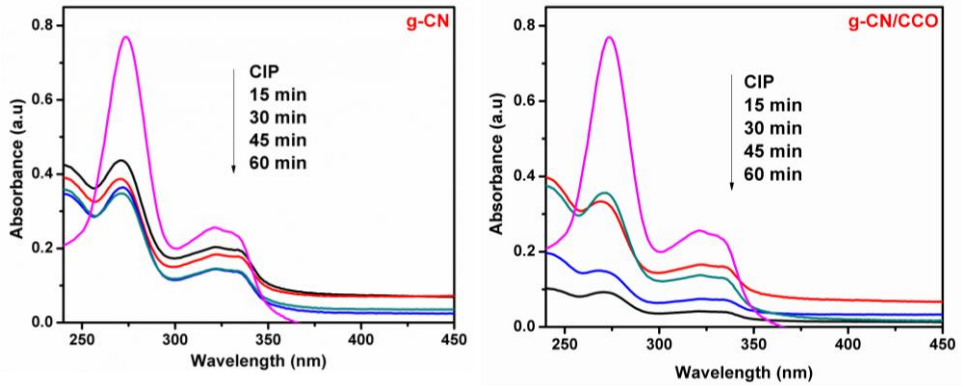

Time(min)	Absorbance	%
15	0.43	43
30	0.38	50
45	0.36	52
60	0.34	55

Time(min)	Absorbance	%
15	0.36	52
30	0.33	56
45	0.14	81
60	0.09	88

Fig.12 Photocatalytic Degradation of CIP: UV-Vis spectra and Degradation Percentages for (a) g-CN and (b) g-CN/CCO Catalysts.

3.3 Plausible Mechanism

Under simulated sunlight irradiation, both g-C_3N_4 and $CuCo_2O_4$ are photoactivated owing to their narrow band gaps and strong visible-light absorption capability. Upon light absorption, electrons in the valence band (VB) of each semiconductor are excited to their respective conduction bands (CB), generating electron–hole pairs. This photoexcitation process initiates charge carrier dynamics at the g-C_3N_4/$CuCo_2O_4$ heterointerface.

Due to the favourable band alignment between the two semiconductors, the photogenerated electrons in the conduction band of g-C_3N_4 tend to migrate toward the conduction band of $CuCo_2O_4$. This electron transfer is driven by the difference in CB energy levels and promotes spatial separation of charge carriers. Meanwhile, the photogenerated holes remain predominantly in the valence band of g-C_3N_4, while some holes may also exist in the VB of $CuCo_2O_4$. This directional charge movement results in effective charge separation, with electrons accumulating in the CB of $CuCo_2O_4$ and holes enriched in the VB of g-C_3N_4, thereby significantly suppressing electron–hole recombination.

The well-separated charge carriers actively participate in surface redox reactions. The accumulated electrons in the CB of $CuCo_2O_4$ react with dissolved molecular oxygen to generate reactive oxygen species such as

superoxide radicals ($O_2^{\bullet-}$), which can further undergo protonation and reduction steps to form hydroperoxyl radicals (•OOH). Simultaneously, the holes present in the VB of g-C_3N_4 possess strong oxidative ability and can oxidize surface-adsorbed water molecules or hydroxide ions to produce highly reactive hydroxyl radicals (•OH).

These generated reactive oxygen species play a crucial role in the photocatalytic degradation of ciprofloxacin (CIP). The ROS attack the CIP molecules through a series of oxidative reactions, leading to the breakdown of the molecular structure, cleavage of functional groups, and eventual mineralization into harmless end products such as CO_2 and H_2O. The synergistic interaction between g-C_3N_4 and $CuCo_2O_4$, combined with efficient charge separation and enhanced ROS generation, accounts for the improved photocatalytic performance of the heterostructure under visible-light irradiation [49]. A picture depicting the plausible mechanism is given in fig. 13.

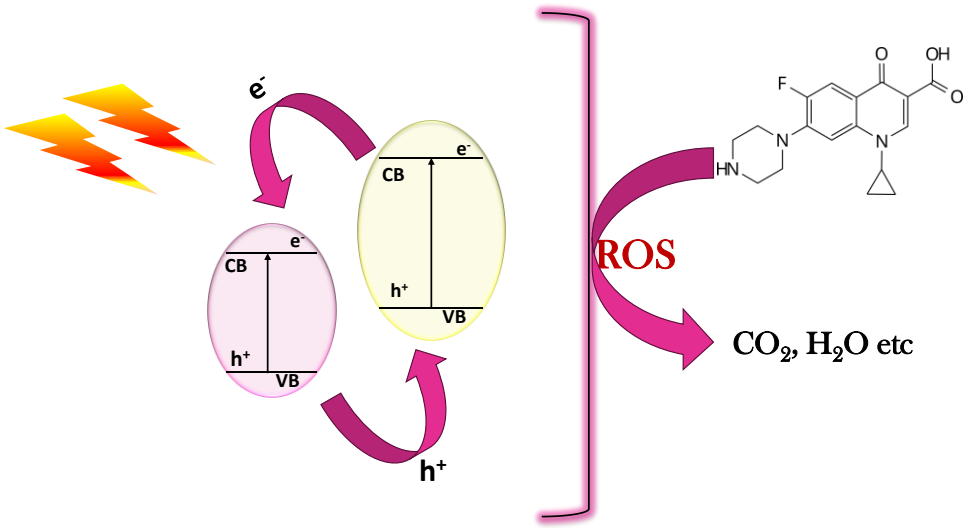

Fig.13 Schematic Representation of Plausible Mechanism: Electron Transfer Facilitating CIP Degradation.

Chapter 4

Conclusions

In this work we have successfully completed the design and fabrication o of g-C_3N_4/CCO heterojunction for enhanced photocatalytic performance. The hybrid g-C_3N_4/CCO heterojunction system was synthesised by an impregnation strategy. FTIR and XRD results substantiates the fine dispersion of CCO over the g-C_3N_4 material. The enhanced absorption in the hybrids was confirmed by UV-DRS plots and the band gap reduction was obtained from Tauc plots. Methylene blue degradation reaction was used as a test reaction for the optimization of precursors. The 1:1 combination of urea and thiourea was found to be the optimized combination for g-C_3N_4 preparation. The hybrid systems were synthesized by employing a wet impregnation method. The as prepared hybrid system was employed for the photocatalytic degradation of a persistent antibiotic CIP. The hybrid systems exhibited enhanced activity for degradation of CIP. The formation of heterostructure resulted in reduced recombination of electron-hole pairs. This enhanced performance of the hybrid systems can be ascribed to the successful formation of heterostructures, which in turn resulted in the efficient charge transfer.

References

1. Patnaik, Sulagna, et al. ‘An Overview of the Structural, Textural and Morphological Modulations of g-C_3N_4 towards Photocatalytic Hydrogen Production’. RSC Advances, vol. 6, no. 52, 2016, pp. 46929–51, https://doi.org/10.1039/C5RA26702A.

2. Hayat, Asif, et al. ‘A Targeted Review of Current Progress, Challenges and Future Perspective of g-C_3N_4 Based Hybrid Photocatalyst Toward Multidimensional Applications’. The Chemical Record, vol. 23, no. 1, Jan. 2023, p. e202200143, https://doi.org/10.1002/tcr.202200143.

3. Fina, Federica, et al. ‘Structural Investigation of Graphitic Carbon Nitride via XRD and Neutron Diffraction’. Chemistry of Materials, vol. 27, no. 7, Apr. 2015, pp. 2612–18, https://doi.org/10.1021/acs.chemmater.5b00411.

4. Darkwah, Williams Kweku, and Yanhui Ao. ‘Mini Review on the Structure and Properties (Photocatalysis), and Preparation Techniques of Graphitic Carbon Nitride Nano-Based Particle, and Its Applications’. Nanoscale Research Letters, vol. 13, no. 1, Nov. 2018, p. 388. Springer Link, https://doi.org/10.1186/s11671-018-2702-3.

5. Zhang, Yuewei, et al. ‘Porous Graphitic Carbon Nitride Synthesized via Direct Polymerization of Urea for Efficient Sunlight-Driven Photocatalytic Hydrogen Production’. Nanoscale, vol. 4, no. 17, Aug. 2012, pp. 5300–03. pubs.rsc.org, https://doi.org/10.1039/C2NR30948C.

6. Zhang, Guigang, et al. ‘Polycondensation of Thiourea into Carbon Nitride Semiconductors as Visible Light Photocatalysts’. Journal of Materials

Chemistry, vol. 22, no. 16, Mar. 2012, pp. 8083–91. pubs.rsc.org, https://doi.org/10.1039/C2JM00097K.

7. Wang, Yong, et al. ‘Facile One-Pot Synthesis of Nanoporous Carbon Nitride Solids by Using Soft Templates’. ChemSusChem, vol. 3, no. 4, Apr. 2010, pp. 435–39, https://doi.org/10.1002/cssc.200900284.

8. Ji, Huanhuan, et al. ‘Photocatalytic Degradation of 2,4,6-Trichlorophenol over g-C_3N_4 under Visible Light Irradiation’. Chemical Engineering Journal, vol. 218, Feb. 2013, pp. 183–90. ScienceDirect, https://doi.org/10.1016/j.cej.2012.12.033.

9. Yan, S. C., et al. ‘Photodegradation Performance of g-C_3N_4 Fabricated by Directly Heating Melamine’. Langmuir, vol. 25, no. 17, Sept. 2009, pp. 10397–401. DOI.org, https://doi.org/10.1021/la900923z.

10. Chang, Wenxi, et al. ‘Highly Efficient H_2 Production over $NiCo_2O_4$ Decorated g-C_3N_4 by Photocatalytic Water Reduction’. Chemical Engineering Journal, vol. 362, Apr. 2019, pp. 392–401. ScienceDirect, https://doi.org/10.1016/j.cej.2019.01.021.

11. Zhurenok, Angelina V., et al. ‘Comprehensive Review on g-C_3N_4-Based Photocatalysts for the Photocatalytic Hydrogen Production under Visible Light’. International Journal of Molecular Sciences, vol. 24, no. 1, Dec. 2022, p. 346, https://doi.org/10.3390/ijms24010346.

12. Suyana, P., et al. ‘Structural and Compositional Tuning in g-C_3N_4 Based Systems for Photocatalytic Antibiotic Degradation’. Chemical Engineering Journal Advances, vol. 8, Nov. 2021, p. 100148. ScienceDirect, https://doi.org/10.1016/j.ceja.2021.100148.

13. Iqbal, Waheed, et al. ‘Controllable Synthesis of Graphitic Carbon Nitride Nanomaterials for Solar Energy Conversion and Environmental Remediation: The Road Travelled and the Way Forward’. Catalysis Science & Technology, vol. 8, no. 18, Sept. 2018, pp. 4576–99. pubs.rsc.org, https://doi.org/10.1039/C8CY01061G.

14. Parga, B., et al. ‘Enhancing Fluorescence Sensing of Metal Species by g-C_3N_4 Prepared by Co-Polymerization of Melamine and Urea Precursors’. Materials Science and Engineering: B, vol. 293, July 2023, p. 116493, https://doi.org/10.1016/j.mseb.2023.116493.

15. Huang, Bin, et al. ‘Review of the Versatility and Application Potentials of g-C_3N_4-Based S-Scheme Heterojunctions in Photocatalytic Antibiotic Degradation’. Molecules, vol. 30, no. 6, Mar. 2025, p. 1240, https://doi.org/10.3390/molecules30061240.

16. Wang, Hao, et al. ‘Highly Crystalline Sulfur-Doped Carbon Nitride as Photocatalyst for Efficient Visible-Light Hydrogen Generation’. Applied Catalysis B: Environmental, vol. 238, Dec. 2018, pp. 592–98, https://doi.org/10.1016/j.apcatb.2018.07.023.

17. Jing, Lin, et al. ‘Effective Prevention of Charge Trapping in Graphitic Carbon Nitride with Nanosized Red Phosphorus Modification for Superior Photo(Electro)Catalysis’. Advanced Functional Materials, vol. 27, no. 46, Dec. 2017, p. 1703484, https://doi.org/10.1002/adfm.201703484.

18. Jiang, Jing, et al. ‘A Comparison Study of Alkali Metal-Doped g-C_3N_4 for Visible-Light Photocatalytic Hydrogen Evolution’. Chinese Journal of Catalysis, vol. 38, no. 12, Dec. 2017, pp. 1981–89, https://doi.org/10.1016/S1872-2067(17)62936-X.

19. Xiong, Peiyao, et al. ‘Alkali Metal Doped Crystalline g-C_3N_4 with an Enriched Cyano Group for Visible-Light Photocatalytic Degradation of Methylamine’. RSC Advances, vol. 13, no. 45, 2023, pp. 31820–34. pubs.rsc.org, https://doi.org/10.1039/D3RA06066G.

20. Ding, Fu, et al. ‘Plasmonic Ag Nanoparticles Decorated g-C_3N_4 for Enhanced Visible-Light Driven Photocatalytic Degradation and H2 Production’. Resources Chemicals and Materials, vol. 1, no. 1, Mar. 2022, pp. 1–7, https://doi.org/10.1016/j.recm.2021.12.004.

21. Xu, Jing, et al. ‘Enhanced Visible-Light-Induced Photocatalytic Degradation and Disinfection Activities of Oxidized Porous g-C_3N_4 by Loading Ag Nanoparticles’. Catalysis Today, vol. 332, July 2019, pp. 227–35, https://doi.org/10.1016/j.cattod.2018.07.024.

22. Xu, Zheng, et al. ‘Waste-to-Energy Conversion on Graphitic Carbon Nitride: Utilizing the Transformation of Macrolide Antibiotics to Enhance Photoinduced Hydrogen Production’. ACS Sustainable Chemistry & Engineering, vol. 5, no. 11, Nov. 2017, pp. 9667–72, https://doi.org/10.1021/acssuschemeng.7b03088.

23. Nguyen Xuan, Truong, et al. ‘Effect of Copper-Modification of g-C_3N_4 on the Visible-Light-Driven Photocatalytic Oxidation of Nitrophenols’. Molecules, vol. 28, no. 23, Nov. 2023, p. 7810, https://doi.org/10.3390/molecules28237810.

24. Dai, Yanhui, et al. ‘Modulation of the Photocatalytic Performance of g-C_3N_4 by Two-Sites Co-Doping Using Variable Valence Metal’. Applied Surface Science, vol. 500, Jan. 2020, p. 144036, https://doi.org/10.1016/j.apsusc.2019.144036

25. Ou, Qi, et al. ‘Porous Visible Light-Responsive Fe^{3+}-Doped Carbon Nitride for Efficient Degradation of Sulfadiazine’. Environmental Science and Pollution Research, vol. 27, no. 22, Aug. 2020, pp. 27849–58. Springer Link, https://doi.org/10.1007/s11356-020-08749-6.

26. Guo, Yanzhen, et al. ‘Favoring Photocatalytic Reactive Species Generation and Utilization Over g-C_3N_4 Nanosheets by Controllable Edge C Modification’. SSRN Electronic Journal, 2022, https://doi.org/10.2139/ssrn.4243335.

27. Guo, Feng, et al. ‘Facile Bottom-up Preparation of Cl-Doped Porous g-C_3N_4 Nanosheets for Enhanced Photocatalytic Degradation of Tetracycline under Visible Light’. Separation and Purification Technology, vol. 228, Dec. 2019, p. 115770, https://doi.org/10.1016/j.seppur.2019.115770.

28. Huang, Jiaxing, et al. ‘An Efficient Metal-Free Phosphorus and Oxygen Co-Doped g-C_3N_4 Photocatalyst with Enhanced Visible Light Photocatalytic Activity for the Degradation of Fluoroquinolone Antibiotics’. Chemical Engineering Journal, vol. 374, Oct. 2019, pp. 242–53, https://doi.org/10.1016/j.cej.2019.05.175.

29. Pattanayak, Dhruti Sundar, et al. ‘Doped Graphitic Carbon Nitride (g-C_3N_4) Catalysts for Efficient Photodegradation of Tetracycline Antibiotics in Aquatic Environments’. Environmental Science and Pollution Research, vol. 30, no. 10, Feb. 2023, pp. 24919–26. Springer Link, https://doi.org/10.1007/s11356-022-19766-y.

30. Nguyen, Thanh-Binh, et al. “Visible-Light Photodegradation of Sulfamethoxazole (SMX) over Ag-P-Codoped g-C_3N_4 (Ag-P@UCN) Photocatalyst in Water.” Chemical Engineering Journal, vol. 384, Mar. 2020, p. 123383, https://doi.org/10.1016/j.cej.2019.123383.

31. Liu, Rui, et al. ‘Design of g-C_3N_4/TiO_2 Nanotubes Heterojunction for Enhanced Organic Pollutants Degradation in Waste Water’. Materials Letters, vol. 251, Sept. 2019, pp. 126–30. ScienceDirect, https://doi.org/10.1016/j.matlet.2019.05.065.

32. Fu, Junwei, et al. ‘g-C_3N_4-Based Heterostructured Photocatalysts’. Advanced Energy Materials, vol. 8, no. 3, Jan. 2018, p. 1701503, https://doi.org/10.1002/aenm.201701503.

33. Xu, Quanlong, et al. ‘Direct Z-Scheme Photocatalysts: Principles, Synthesis, and Applications’. Materials Today, vol. 21, no. 10, Dec. 2018, pp. 1042–63, https://doi.org/10.1016/j.mattod.2018.04.008.

34. Fan, Yanyun, et al. ‘$NiCo_2O_4$/g-C_3N_4 Heterojunction Photocatalyst for Efficient H_2 Generation’. Energy Technology, vol. 9, no. 5, May 2021, p. 2000973, https://doi.org/10.1002/ente.202000973.

35. Gu, Jing-wen, et al. ‘Construction of Full Spectrum-Driven Cs_xWO3/ g-C_3N_4 Heterojunction Catalyst for Efficient Photocatalytic CO_2 Reduction’. Applied Surface Science, vol. 540, Feb. 2021, p. 148316, https://doi.org/10.1016/j.apsusc.2020.148316.

36. Li, Liang, et al. ‘Boosting Charge Separation and Photocatalytic CO_2 Reduction of $CsPbBr_3$ Perovskite Quantum Dots by Hybridizing with P_3HT’. Chemical Engineering Journal, vol. 419, Sept. 2021, p. 129543. ScienceDirect, https://doi.org/10.1016/j.cej.2021.129543.

37. Wang, Xuewen, et al. ‘3D Macropore Carbon-Vacancy g-C_3N_4 Constructed Using Polymethylmethacrylate Spheres for Enhanced Photocatalytic H_2 Evolution and CO_2 Reduction’. Journal of Energy Chemistry, vol. 53, Feb. 2021, pp. 139–46. ScienceDirect, https://doi.org/10.1016/j.jechem.2020.05.001.

38. Wu, Chunzheng, et al. ‘Making g-C_3N_4 Ultra-Thin Nanosheets Active for Photocatalytic Overall Water Splitting’. Applied Catalysis B: Environmental, vol. 282, Mar. 2021, p. 119557, https://doi.org/10.1016/j.apcatb.2020.119557.

39. Tian, Bin, et al. ‘Metal-Free Plasmonic Boron Phosphide/Graphitic Carbon Nitride with Core-Shell Structure Photocatalysts for Overall Water Splitting’. Applied Catalysis B: Environmental, vol. 280, Jan. 2021, p. 119410, https://doi.org/10.1016/j.apcatb.2020.119410.

40. Zhao, Hui, et al. ‘Photo-Assisted Separation of Noble-Metal-Free Oxidation and Reduction Cocatalysts for Graphitic Carbon Nitride Nanosheets with Efficient Photocatalytic Hydrogen Evolution’. Applied Catalysis B: Environmental, vol. 280, Jan. 2021, p. 119456, https://doi.org/10.1016/j.apcatb.2020.119456.

41. Jeghan, Shrine Maria Nithya, et al. ‘Fabrication of Flower-like Copper Cobaltite/Graphitic-Carbon Nitride ($CuCo_2O_4$/g-C_3N_4) Composite with Superior Photocatalytic Activity’. Journal of Industrial and Engineering Chemistry, vol. 57, Jan. 2018, pp. 405–15, https://doi.org/10.1016/j.jiec.2017.08.049.

42. Ali, Yasir, et al. ‘Challenges, Prospects, and Surface Chemistry of $CuCo_2O_4$ in Energy Storage, Electro-Photocatalysis, Solar Cells, and Sensor Applications’. Journal of Materials Science: Materials in Electronics, vol. 36, no. 19, July 2025, p. 1189, https://doi.org/10.1007/s10854-025-15230-y.

43. Giri, Ardhendu Sekhar, and Animes Kumar Golder. ‘Ciprofloxacin Degradation in Photo-Fenton and Photo-Catalytic Processes: Degradation Mechanisms and Iron Chelation’. Journal of Environmental Sciences, vol.

80, June 2019, pp. 82–92. ScienceDirect, https://doi.org/10.1016/j.jes.2018.09.016.

44. Gauba, Pammi, and Arushi Saxena. ‘Ciprofloxacin Properties, Impacts, and Remediation’. CABI Reviews, Feb. 2023, p. cabireviews.2023.0005, https://doi.org/10.1079/cabireviews.2023.0005.

45. Ezhumalai, Yamuna, et al. ‘Graphite Carbon Nitride’. Photocatalysts - New Perspectives, IntechOpen, 2022. www.intechopen.com, https://doi.org/10.5772/intechopen.104976.

46. Sun, Mengxuan, et al. ‘Co-Precipitation Synthesis of $CuCo_2O_4$ Nanoparticles for Supercapacitor Electrodes with Large Specific Capacity and High-Rate Capability’. Electrochimica Acta, vol. 397, Nov. 2021, p. 139306. ScienceDirect, https://doi.org/10.1016/j.electacta.2021.139306.

47. Al-Aqeel, Muneerah. ‘Liquid-Free Simple Synthesis of Nickel Cobaltite Nanostructures for High-Performance Supercapacitors and Electrocatalyst Applications’. Journal of Solid-State Electrochemistry, vol. 29, no. 12, Dec. 2025, pp. 5225–32. Springer Link, https://doi.org/10.1007/s10008-025-06367-1.

48. Khan, Idrees, et al. ‘Review on Methylene Blue: Its Properties, Uses, Toxicity and Photodegradation’. Water, vol. 14, no. 2, Jan. 2022, p. 242, https://doi.org/10.3390/w14020242.

49. Joseph, Merin, et al. ‘Heterojunction Engineering of g-C_3N_4 with CuO for Enhanced Photocatalytic and Photoelectrochemical Performance’. Energy Technology, vol. 12, no. 4, Apr. 2024, p. 2301340, https://doi.org/10.1002/ente.202301340.